Digital current regulator for proportional electro-hydraulic valves featuring unknown disturbance rejection

To appear in ISA Transactions, DOI: 10.1016/j.isatra.2013.08.013

Digital current regulator for proportional electro-hydraulic valves featuring unknown disturbance rejection

Enrico Canuto[1], Wilber Acuña-Bravo[1], Marco Agostani[2] and Marco Bonadei[2]

[1]Politecnico di Torino, Dipartimento di Automatica e Informatica

Corso Duca degli Abruzzi 24, 10129 Torino, Italy

enrico.canuto@polito.it, wilber.acunabravo@polito.it

[2]Atos SpA, Via alla Piana 57, Sesto Calende, Italy

magostani@atos.com, mbonadei@atos.com

Contact author

Enrico Canuto

Politecnico di Torino, Dipartimento di Automatica e Informatica

Corso Duca degli Abruzzi 24, 10129 Torino, Italy

e-mail: enrico.canuto@polito.it

tel. +39 011 090 7026

fax +39 011 090 7099

ABSTRACT

Solenoid current regulation is well-known and standard in any proportional electro-hydraulic valve. The goal is to provide a wide-band transfer function from the reference to the measured current, thus making the solenoid a fast and ideal force actuator within the limits of the power supplier. The power supplier is usually a Pulse Width Modulation (PWM) amplifier fixing the voltage bound and the Nyquist frequency of the regulator. Typical analogue regulators include three main terms: a feedforward channel, a proportional feedback channel and the electromotive force compensation. The latter compensation may be also accomplished by

integrative feedback. Here the problem is faced through a model-based design (Embedded Model Control), on the basis of a wide-band embedded model of the solenoid which includes the effect of eddy currents. To this end model parameters must be identified. The embedded model includes a stochastic disturbance dynamics capable of estimating and correcting the electromotive contribution together with the model parametric uncertainty, variability and state dependence. The embedded model which is fed by the measured current and the supplied voltage becomes a state predictor of the controllable and disturbance dynamics. The control law combines a reference generator, state feedback and disturbance rejection to dispatch the PWM with the appropriate duty cycle. Modeling, identification and control design are outlined together with experimental result. Comparison with an existing analogue regulator is also provided.

KEYWORDS：Current regulator, disturbance rejection, identification, solenoid, model-based control

1 Introduction

1.1 Goal and rationale of the paper

Solenoid current regulation of proportional electro-hydraulic valves appears to be a standard and mature control problem [1]. To the authors' knowledge, few scientific papers [2] have been recently devoted to the subject, whereas tens of integrated circuits and boards are available on the market. Nowadays, major emphasis is directed toward current regulators of small synchronous motors [3], [4], [5], AC drives [6], [7] and automotive applications [8], [9], [10]. This paper aims to design a solenoid digital current regulator, aided by a model–based design methodology like the Embedded Model Control (EMC) [11], [12], and to assess the experimental results in comparison with an existing analogue regulator. The 100 W solenoid under study drives an off-the-shelf proportional electro-hydraulic valve. The solenoid is driven by a 24 V Pulse Width Modulation (PWM) amplifier switching at 10 kHz. The input signals of

the current regulator are the digital output of a milliampere-accurate current sensor and the current reference provided by the valve position control [13], acting as the outer loop of a hierarchical controller. Unlike moving coil motors, solenoids only provide a unidirectional force (in this case of the order of 100 N) which is contrasted by a spring assembly. Thus the current must be regulated around a variable current bias (about 1.6 A) so as to withstand the spring reaction force at the zero position of the useful valve stroke. Besides current bias, solenoid current regulation encounters targets and constraints that are typical of electric drives [1]: wide bandwidth (BW), large slew rate, bounded supply voltage, magnetic hysteresis, variable inductance, resistance and electromotive force, power amplifier delay, eddy currents if the magnetic circuit is not laminated which is the case of valve solenoids.

Current regulators of electric drives usually include a feedforward command, a proportional feedback, a direct compensation of the electromotive force and of the solenoid resistance variation [10]. As an alternative to direct compensation, proportional and integrative (PI) feedback is used [1], [4], [6], but the PI feedback must be equipped with an anti-windup strategy to withstand supply voltage saturation [14]. The design of digital regulators is often approached by converting continuous time to discrete time [6], [8]. Direct discrete-time design can account for transport delays as in [14]. Very often simple algorithms are preferred because of a limited computing time.

Here a discrete-time (digital) model-based design as suggested by the Embedded Model Control (EMC) is applied to a valve solenoid. Advantages of an EMC regulator are the following.

1) An accurate model of the solenoid dynamics and of the PWM response is made available, included in the control algorithm (it will be referred to as the embedded model), and it may be tailored and tuned to a specific solenoid class. The model may be pushed by identification to include PWM and sensor delays, as well as eddy current dynamics [15] close to the PWM Nyquist frequency $f_{\max} = 5$ kHz . An identification algorithm has been designed and tested on purpose. In fact, a mere chain of integrators as suggested by Active Disturbance Rejection Control (ADRC, [16], [17]) does not fit, since eddy

currents make the solenoid dynamics of fractional order, and delays are added by PWM and sensor electronics.

2) The control algorithm features automatic rejection of parametric uncertainty and variability (for instance, the resistance drift due to temperature [18]) as well as of external disturbances like the electromotive force. Rejection is designed so as to avoid supplementary measurements (solenoid temperature, plunger velocity) and integrative actions. This is achieved by completing the embedded model with a stochastic dynamics capable of updating the disturbance state within a wide frequency band, which is only limited by sensor noise and neglected dynamics. Disturbance estimation and rejection of unknown disturbances (including parametric uncertainty) is an effective procedure that is usually dealt with the aid of a state observer [19], [20]. Here as in other applications of the EMC [21], [22], the concept and practice of the embedded model is exploited for building up a real-time model of the plant and disturbances, which is capable of being continuously updated, and can therefore provide the right information (state variables) to the control law.

3) EMC disturbance observers appear to be different from ADRC. The latter observers are built around a high-frequency model of the controllable dynamics taking the form of a chain of integrators, whose size matches the input-output relative degree (denominator less numerator degree, here of fractional order). A further integrator is included, the output playing the role of input disturbance. A static output-to-state feedback as in Kalman filters is drawn from the output error (the same as the EMC model error) to the input of each integrator and the feedback gains are tuned for guaranteeing stability and bandwidth just on a model basis. On the contrary, EMC assumes that the embedded model is perturbed at higher frequencies by a neglected dynamics, which increases the model relative degree to the detriment of the overall stability and performance. The observer eigenvalue tuning in Section 3.3 has been proved by EMC (ref. [11], [12]) to be the key tool for blocking neglected dynamics and high-frequency uncertainty from entering feedback and destabilizing the whole closed-loop system. For instance,

uncertainty in the high-frequency gain (the sole model parameter in the ADRC case) may be so large as to require a wide BW, which may conflict with the upper limit imposed by the neglected dynamics and render control design unfeasible, as pointed out in Section 3.3. Further design issues that are solved by EMC are: (i) delays cannot be treated as integrators, which suggests direct discrete-time design, (ii) the observer feedback variables are treated as noise components (Section 2.3) to be designed together with the disturbance dynamics, (iii) disturbance dynamics must be given the right state equation (not necessarily of the first order) which is capable of describing the class of the plant uncertainty to be rejected, (iv) the disturbance entry points in the controllable dynamics may be everywhere, which requires a specific disturbance rejection law as in Section 3.4.

4) Driving the embedded model with the same command which is dispatched to the plant, eliminates any integral windup when the command saturates. The reason is that the disturbance state of the embedded model is continuously updated by the residual discrepancy between plant and model running under the same command. As a result the EMC control law in Section 3.4, unlike PID feedback laws, becomes static, the only state variable being a delay between pre-computed and current command. The reference generator in Section 3.2 provides a reference duty cycle and reference state variables that are coherent with the duty-cycle range. In this manner, contribution to command saturation of tracking errors and disturbance rejection is minimized.

5) The overall input-output dynamics is shaped for meeting the requirements in Section 3.1. This is achieved by eigenvalue tuning as shown in Sections 3.3 and 3.4.

6) Last but not least, the current regulator fits into the hierarchical control scheme of a valve position control [13], since it receives the reference current $\underline{I}$ from the position control and provides the latter control with current and current derivatives (Figure 1).

Figure 1 Current regulator and position control.

The goal of a current regulator is to convert solenoids into ideal force actuators of position controllers. In other words, a current regulator becomes the inner loop of a position control loop

as in Figure 1. In view of a position bandwidth wider than 100 Hz, a milliampere-accurate repeatability of the current reference $\underline{I}$ is demanded from DC to about 1 kHz. The regulator is fed by a current reference $\underline{I}$, generated by the position controller, and must guarantee fast and accurate tracking of the reference current within the limits of the PWM amplifier, i.e. voltage bound, $|V| \le V_{\max} = 24$ V, and delay.

Three main performance indices characterize a solenoid current regulator.

1) The first is the slew rate $(dI/dt)_{\max}$ in response to reference steps. The slew rate is limited by the PWM voltage $V_{\max}$ and by the self-inductance. It may be identified and assessed from the response to a square-wave reference.
2) The second is the tracking delay in the linear response region. It may be identified and assessed either by the harmonic response or by the time response to canonical reference signals.
3) The third is the accuracy of the tracking error to be measured under steady state and transient conditions.

The paper starts in Section 2 with a discrete-time dynamic model and the relevant identification procedure. Fine and simplified models are discussed to fix the embedded model of the control algorithm. The current regulator is outlined in Section 3. This is the combination, in accordance with the EMC, of a reference generator, state predictor and control law. The state predictor, made by embedded model and noise estimator, is essential to estimate the unknown disturbance to be rejected. The attribute 'unknown' emphasizes the fact that no supplementary measurements are necessary to the purpose. Experimental tests prove the regulator performance and show the advantage of the proposed disturbance rejection. Formulation is reduced to a minimum.

2 Solenoid dynamic model and identification

2.1 Model class

The goal is to identify a discrete-time state equation which is driven by the PWM duty cycle $-1 \le u \le 1$ and by the measurable plunger speed $v = \dot{x}$ [m/s], and provides the measurable

solenoid current I [A] as output. The time unit $T = 0.1$ ms is dictated by the PWM cycle. Due to a complex magnetic circuit, magnetic flux saturation and solenoid heating, the equation parameters collected in the vector $\mathbf{p}(I,x,t)$ depend on the current I, on the plunger position x and are time varying. By expressing them as the sum of a mean (nominal) value $\underline{\mathbf{p}}$ and of an uncertain but bounded deviation $\delta\mathbf{p}(I,x,t)$, a linear time-invariant state equation can be written as follows

$$\begin{aligned} &\mathbf{x}(i+1) = A(\underline{\mathbf{p}})\mathbf{x}(i) + B(\underline{\mathbf{p}})u(i) + G(\underline{\mathbf{p}})v(i) + \mathbf{h}(\mathbf{x},u;\underline{\mathbf{p}},\delta\mathbf{p}),\ \mathbf{x}(0) = \mathbf{x}_0 \\ &y(i) = C\mathbf{x}(i) + e(i) = y_m(i) + e_m(i) \\ &|\delta\mathbf{p}| \le \delta p_{\max} \end{aligned}, \qquad (1)$$

where the model output y_m, the measured output y and the model error e_m are indicated. In (1), $\mathbf{h}(\cdot)$ is a static vectorial function accounting for the effect of $\delta\mathbf{p}$ on the state vector $\mathbf{x}$. $\mathbf{h}$ and $\delta\mathbf{p}$ are assumed to be continuous in all the arguments. One of the current regulator goals is to predict and reject $\mathbf{h}(\cdot)$ by means of the control signal u in the same way as an unknown input disturbance. The model error $e_m = y - y_m$, in the linear domain, can be written as the sum of the measurement noise w_y and of the effect of the high-frequency dynamics (mainly eddy currents) that have been neglected in (1). The corresponding equation is

$$e_m = w_y + \partial P \cdot y_m, \qquad (2)$$

where the dynamic operator ∂P is referred to as the fractional model error. By taking the Z-transform of (2), it is shown in [11] that $\left|\partial P\left(e^{j\omega T}\right)\right|$ tends to increase at higher frequencies and often overcomes the unit value, which corresponds to a 100% model error at an angular frequency ω. Model identification should tend to bound $\left|\partial P\left(e^{j\omega T}\right)\right|$ below unit. The goal can be achieved by increasing the model order, i.e. the state vector dimension, but at the cost of a larger parametric uncertainty. In the case $\max_\omega \left|\partial P\left(e^{j\omega T}\right)\right| > 1$, the state predictor of the control unit (the ensemble of embedded model and noise estimator) is in charge of abating, with some margin [11], the fractional error overshoot to below unit. This task is one of the key design techniques of the EMC.

Previous discussions can be summarized by saying that the model uncertainty can be split into two main terms: (i) parametric uncertainties entering the static function $\mathbf{h}(\cdot)$ and affecting the model state variables through (1), (ii) the neglected dynamics ∂P affecting the model output. Both uncertainties must be accounted for and accommodated by the control design, less instability and performance degradation.

Nominal model and deviations as formulated in (1) have been identified in two stages.

1) A large-signal identification provides the nominal parametric model to be embedded in the control system.
2) A small-signal identification around a current value and at a fixed plunger position provides the harmonic response to be compared with the parametric model.

Experimental data are shown in Figure 2 and Figure 3 up to the Nyquist frequency $f_{\max}$. The dashed responses have been obtained with a small sinusoidal duty cycle (± 0.025) around a bias fixing the mean current in the range $I_{\text{mean}} = 1 \div 3$ A. The solid response has been obtained by the parametric identification excited by a pseudo-random duty cycle which is ten times larger (± 0.25) and varies around the zero position bias. Harmonic response variations are rather significant, fairly uniform for $f > 10$ Hz, and are mainly due to a variable inductance because of the magnetic circuit saturation. The relative variation has been estimated close to $\pm 20\%$. To avoid nonlinear terms in (1), inductance variation and uncertainty have been accounted for by $\mathbf{h}(\cdot)$.

Figure 2 Magnitude of the harmonic response.

Figure 3 Argument of the harmonic response.

Both diagrams in Figure 2 and Figure 3 show the effect of the solenoid eddy currents and of the PWM delay, since the magnitude plot decays less than -20 dB/dec at $f > 10$ Hz, and the argument remains close to -1 rad before abruptly decaying and repeating the delay argument

shape. The corresponding transfer function is not rational, but within a finite frequency band can be approximated by a rational function with zeros and poles having relative degree $r=1$. The goal of the parametric identification in Section 2.2 was to identify such an approximation up to $f_{\max}$. Identifying the electrical parameters of the eddy current dynamics was not the goal [15].

Typical eigenvalues of the open-loop dynamics (1), together with control system eigenvalues, are reported in Table I.

2.2 Parametric identification

Parametric identification is based on the ARX model [24] of (1). To this end, (1) is rewritten in the form of a transfer function as follows

$$\begin{aligned} I(z) &= \frac{B(z)}{A(z)}u(z)+\frac{G(z)}{A(z)}v(z)+\frac{d(z)}{A(z)} \\ y(z) &= \left(1+\partial P(z)\right)I(z)+w_y(z)=y_m(z)+e_m(z) \end{aligned}, \tag{3}$$

where A, B and G are different from (1) and hold

$$\begin{aligned} A(z) &= z\left(z^n+a_{n-1}z^{n-1}+\ldots+a_1z+a_0\right) \\ B(z) &= b_mz^m+\ldots+b_1z+b_0 \\ G(z) &= g_mz^m+\ldots+g_1z+g_0 \end{aligned}. \tag{4}$$

In (3), $y(z)$ is the current measurement, $e_m(z)$ is the model error, $v(z)$ is the velocity measurement, and $d(z)$ is a disturbance term which includes the components of $\mathbf{h}(\cdot)$ in (1) that cannot enter a linear model. The degree n has been selected to be $n=3$ to reduce the model order to a minimum, while keeping the fractional model error less than unit, i.e. $\left|\partial P\left(e^{j\omega T}\right)\right|<1$. The numerator degree holds $m=2$, and the relative degree holds $r=n+1-m=2$, because of a delay fitting the argument as in Figure 3. By separating model and neglected dynamics, one obtains the following ARX form [24], [25], [26]:

$$\begin{aligned} A(z)y(z) &= B(z)u(z)+G(z)v(z)+\eta(z) \\ \eta(z) &\cong d(z)-A(z)\partial P(z)y(z) \end{aligned}, \tag{5}$$

where y, u and v are known, η is unknown, and the sensor noise w_y in (2) has been dropped because rather negligible at higher frequencies (see the bottom curve in Figure 4). The ARX form (5) assumes that η is a white noise. The assumption has been verified from experimental data.

Figure 4 Spectral density of the normalized duty cycle (top), of the measured current (decreasing curve), of the residuals (middle) and of the sensor noise (bottom).

The solenoid has been excited by a pseudo-random duty cycle whose spectral density (PSD) is top curve of Figure 4. The duty cycle u has been normalized to be a current I_u through the equality

$$I_u = uB(z=1)/A(z=1) = K_0 u = \frac{V_{\max}}{R} u \cong 5.7u\,, \tag{6}$$

where R is the solenoid resistance. Figure 4 shows also the PSD of the measured current y and of the residual η. Residuals (the middle curve in Figure 4) look rather close to being white, which is a key assumption of the ARX model (5). At lower frequencies, they repeat the driving input because of identification errors in the low frequency gain K_0 in (6). At mid and higher frequencies they slightly deviate from a flat profile, which is typical of a white noise, because of the neglected dynamics ∂P. The current PSD decreases less than -20 dB/dec as expected.

2.3 The embedded model

To compensate for the parametric uncertainty which is accounted in (1) by the term $\mathbf{h}$, the embedded model is completed with a disturbance dynamics capable of surrogating $\mathbf{h}$. A stochastic disturbance class $\mathcal{D}$ whose realization is denoted by the vector $\mathbf{d}(i)$, $n\times 1$, replaces the unknown vector $G(\underline{\mathbf{p}})v(i)+\mathbf{h}(\cdot)$ in (1), where $G(\underline{\mathbf{p}})v(i)$ may be treated either as known or unknown. The disturbance class has been designed to be the combination of a white noise and a random drift, as in the following equation

$$\begin{aligned} &x_d(i+1) = x_d(i) + w_d(i),\ x_d(0) = x_{d0} \\ &\mathbf{d}(i) = Hx_d(i) + N\mathbf{w}(i) \end{aligned}, \tag{7}$$

whose matrices and vectors are:

$$\begin{aligned} \mathbf{w}^T &= \begin{bmatrix} w_3 & w_2 & w_1 & w_0 \end{bmatrix} \\ H^T &= \begin{bmatrix} h_3 & h_2 & h_1 & h_0 \end{bmatrix} \\ N &= \operatorname{diag}\{n_3, n_2, n_1, n_0\} \end{aligned} . \tag{8}$$

The following Lemma is straightforward.

Lemma 1. The state equation (7) gives rise to the following Z-transform in (3)

$$d(z) = \frac{h_3 z^3 + h_2 z^2 + h_1 z + h_0}{z-1} w_d(z) + n_3 z^3 w_3(z) + n_2 z^2 w_2(z) + n_1 z w_1(z) + n_0 w_0(z) . \square \tag{9}$$

As expected, $d(z)$ is the sum of a white noise combination (the last four terms) and a drift. The white noise part is coherent with the identification results in Section 2.2, showing that the PSD of the identification residual η (including d) is close to being flat. The drift term aims to model the components of $\mathbf{h}\left(\mathbf{x}(i), u(i); \underline{\mathbf{p}}, \delta\mathbf{p}(i)\right)$ that have not been identified: typically parameter variations like the solenoid resistance thermal variation. Actually, the size n_d of x_d in (7) should be a matter of design, and experimental comparisons between different orders should be the right procedure. Here $n_d = 1$ has been selected for the sake of simplicity, relying on the fact that a current regulator is an inner loop of a hierarchical control, whose outer loop (the position control) is capable of rejecting low-frequency residuals of the inner loop. A further reason is that a first-order dynamics replaces the integrative action of a PI current regulator, and eliminates, as already mentioned, integral wind-up. Unlike PI regulators, which are in charge of zeroing both reference and disturbance static errors, equation (7) is only in charge of fitting disturbance and parametric uncertainty. Reference errors are eliminated by a specific reference generator.

The embedded model is obtained by combining (1) and (7). The total state size is $n = 5$. The state vector is partitioned into controllable state $\mathbf{x}$ and disturbance state x_d. The model equation, written in a compact form, is the following

$$\begin{bmatrix} \mathbf{x} \\ x_d \end{bmatrix}(i+1) = \begin{bmatrix} A & H \\ 0 & 1 \end{bmatrix}\begin{bmatrix} \mathbf{x} \\ x_d \end{bmatrix}(i) + \begin{bmatrix} B \\ 0 \end{bmatrix}u(i) + \begin{bmatrix} N & 0 \\ 0 & 1 \end{bmatrix}\begin{bmatrix} \mathbf{w} \\ w_d \end{bmatrix}(i) + \begin{bmatrix} G \\ 0 \end{bmatrix}v(i)$$
$$y(i) = \begin{bmatrix} C & 0 \end{bmatrix}\begin{bmatrix} \mathbf{x} \\ x_d \end{bmatrix}(i) + e(i) = y_m(i) + e(i), \ \begin{bmatrix} \mathbf{x} \\ x_d \end{bmatrix}(0) = \begin{bmatrix} \mathbf{x}_0 \\ x_{d0} \end{bmatrix} \tag{10}$$

The parameters of A, B and G are those estimated in Section 2.2. In (10), y_m is the model output, free of the model error e_m. The controllable state vector $\mathbf{x}$ in (10) is the following

$$\mathbf{x}^T = \begin{bmatrix} x_3 & x_2 & x_1 & x_0 \end{bmatrix} \tag{11}$$

The upmost three components of $\mathbf{x}$, namely x_k, $k = 0,1,2$ account for solenoid and eddy currents, x_0 accounts for PWM delay. The matrices in (10), that are not reported in (7), derive from (4) and read as follows

$$A = \begin{bmatrix} -a_3 & 1 & 0 & 0 \\ -a_2 & 0 & 1 & 0 \\ -a_1 & 0 & 0 & 1 \\ 0 & 0 & 0 & 0 \end{bmatrix}, \ A_d = 1, \ B = \begin{bmatrix} 0 \\ b_2 \\ b_1 \\ b_0 \end{bmatrix}, \ G = \begin{bmatrix} 0 \\ g_2 = 0 \\ g_1 \\ g_0 = 0 \end{bmatrix}, \ C = \begin{bmatrix} 1 & 0 & 0 & 0 \end{bmatrix}. \tag{12}$$

The zero entries of G and B are a result of the parametric identification. The following lemma is straightforward.

Lemma 2. Equation (10) with the matrices in (12) is controllable by u and observable by y. □

What remains to be found are the coefficients of H and N, since they give form to the interaction between the uncertainty model (7) and the controllable dynamics. The step corresponds to the 'noise design' in [27], which may be retained as a peculiarity of EMC. The design aims at a simple and meaningful interaction form. Let us begin with H that couples the drift state with $\mathbf{x}$. The aim is to correct the variability of the DC gain K_0 in (6) through Hx_d. To this end, H should be proportional to B. Actually H has been simplified to be proportional to G. Besides a sake of simplicity, B turns to possess three non-zero coefficients only because two of the four eigenvalues of A are close to zero, as shown in Table 1. Were both delays neglected, A would reduce to a second-order matrix and B to a single

non zero coefficient equal to $b_0 + b_1 + b_2$, which justifies the single non-zero coefficient of H. The coefficient, being x_d arbitrary, is set equal to one. Simplification of H is balanced by fixing all the coefficients of N to be non-zero, except the last one, $n_0 = 0$. Again, the last two noise terms in (8), w_1 and w_0, can substitute each other being just separated by a delay. At the end, H and N become

$$\begin{aligned} H^T &= \begin{bmatrix} 0 & 0 & 1 & 0 \end{bmatrix} \\ N &= \operatorname{diag}\{1,1,1,0\} \end{aligned}. \tag{13}$$

The block-diagram of the embedded model is shown in Figure 5. Clouds denote uncertainty sources.

Figure 5 Block diagram of the embedded model.

3 Current regulator design

3.1 Requirements

The goal is to design a dead-beat control, meaning that the close loop dynamics in the linear domain must approximate a delay chain driven by the reference current $\underline{I}$ and the tracking error $\underline{e}$, i.e.

$$\begin{aligned} &I(t) = \underline{I}(t-\tau) + \underline{e}(t), \ \tau \le 0.3 \text{ ms} \\ &\mathcal{E}\{\underline{e}(t)\} = 0, \ |\underline{e}(t)| \le 1.5 \text{ mA} \end{aligned}. \tag{14}$$

The bound on the delay τ is imposed by the relative degree $n+1-m=2$ in (10), plus a margin delay. The bound on the tracking error $\underline{e}$ is obtained by fixing a bounded contribution $|\Delta e_x| \le 5\ \mu\text{m}$ to the valve position tracking error. In the frequency band of the spool-spring resonance (50 Hz), such a contribution can be written as

$$|\Delta e_x| \cong \frac{\phi}{K}|\underline{e}| \cong 0.0035|\underline{e}|, \tag{15}$$

where ϕ [Vs/m] is the solenoid force constant and K [N/m] is the spring stiffness. The linear domain is defined by the bounds

$$\begin{aligned} 0 \le \underline{I} \le \underline{I}_{\max} = 3 \text{ A} \\ -1 \le u \le 1 \end{aligned} . \tag{16}$$

In the linear domain the deadbeat control is optimal for what concerns the magnitude $\underline{H}(j\omega) = 1$ of the input-output transfer function $H(s) = I(s) / \underline{I}(s)$, since the reference signal $\underline{I}$ is repeated without distortion after a delay τ, less a zero-mean and random tracking error $\underline{e}$. In principle optimization might also address the delay τ and the variance $\underline{\sigma}_e^2$ of the tracking error. Actually they are imposed by higher level requirements or by the embedded model structure as previously outlined.

The duty cycle limit in (16) fixes the current slew-rate through the PWM voltage $V_{\max}$, the voltage bias $V_0 \cong 6$ V contrasting the spring force, and the inductance L. Due to the voltage bias, different slew rates correspond to positive and negative voltage jumps, namely

$$\begin{aligned} \left(\frac{dI}{dt} \right)_{+,\max} \le \frac{V_{\max} - V_0}{L} \approx 360 \ \frac{\text{A}}{s} \\ \left(\frac{dI}{dt} \right)_{-,\max} \le \frac{V_{\max} + V_0}{L} \approx 640 \ \frac{\text{A}}{s} \end{aligned} . \tag{17}$$

The regulator architecture is the assembly of the following subsystems, which are typical of the Embedded Model Control [11]. They are (i) the reference generator, (ii) the state predictor and (iii) the control law. The current regulator block-diagram is in Figure 6. The box marked with D denotes a delay, i.e. a memory saving the one-step anticipated command before dispatching.

Figure 6 Current regulator block-diagram.

3.2 Regulator architecture: the reference generator

The reference generator provides the open-loop command $\underline{u}$ that drives the state $\underline{\mathbf{x}}$ of a nominal model to the desired current $\underline{I}$. The reference generator is derived from the ARX equation (5) by setting $\eta(z) = 0$, and including the plunger velocity v_r, which is not

compulsory because of the disturbance state x_d in (7). In this way the electromotive force may be accounted for either explicitly or not. Rewriting (5) as a difference equation and solving for the most recent duty cycle occurring at time $i-1$, one obtains the reference command equation:

$$\begin{aligned} u_r(i-1) &= -\frac{1}{b_2}\left(b_1 u_r(i-2) + b_0 u_r(i-3) + g_1 v_r(i-2)\right) \\ &+ \frac{1}{b_2}\left(\underline{I}(i+1) + a_3\underline{I}(i) + a_2\underline{I}(i-1) + a_1\underline{I}(i-2)\right) \\ -1 &\le u_r(i-1) \le 1 \end{aligned} \quad . \tag{18}$$

Underlined symbols in (18) denote reference variables. Equation (18) implements a causal inverse of the embedded model (10), but free of unknown input signals. During the computing step i, $iT \le t < (i+1)T$, the current prediction $\underline{I}(i+1)$ is assumed to be made available by the valve position control within the current limits (16). The reference vector $\mathbf{x}_r$ of the state vector $\mathbf{x}$ in (11), which is employed by the control law in Section 3.4, is obtained by solving the state equation in (10). The equation is excited by the past sequence $u_r(i-k),\ k \ge 2$ of the duty cycles and by the past sequence of the plunger velocity $v_r(i-k),\ k \ge 2$ as follows

$$\begin{aligned} \mathbf{x}_r(i-1) &= A\mathbf{x}_r(i-2) + Bu_r(i-2) + Gv_r(i-2) \\ \mathbf{x}_r &= \begin{bmatrix} x_{r3} \\ x_{r2} \\ x_{r1} \\ x_{r0} \end{bmatrix} \end{aligned} \quad . \tag{19}$$

The reference generator has no parameter to be tuned, and the reference state accounts for the duty-cycle saturation. Since $u_r(i-1)$ and $\mathbf{x}_r(i-1)$ are exogenous variables of the current regulator, they are two-step anticipated in order to define the reference variables

$$\underline{u}(i+1) = u_r(i-1),\ \underline{\mathbf{x}}(i+1) = \mathbf{x}_r(i-1) \tag{20}$$

which are employed by the control law in Section 3.4.

3.3 Regulator architecture: the state predictor

3.3.1 State predictor equations

The state predictor is the ensemble of the embedded model (10) and of the noise estimator in charge of estimating in real-time the unknown noise vector $\mathbf{w}(i)$ that has been defined in (11) . Noise design in Section 2.3 has suggested that the noise size be $n_w = n-1 = 4$, as it allows a static noise estimator to be employed [27]. It holds

$$\begin{aligned} \bar{\mathbf{w}}(i) &= L\left(y(i) - \hat{y}_m(i)\right) \\ L^T &= \begin{bmatrix} l_3 & l_2 & l_1 & l_d \end{bmatrix} \end{aligned}, \tag{21}$$

where the 'bar' denotes estimated variables depending on the present and past output values, namely $y(i-k),\ k \geq 0$. On the contrary, 'hat' denotes one-step prediction only depending on the past values $y(i-k),\ k > 0$. The gains of L are tuned by fixing $n_w = 4$ real-valued closed-loop eigenvalues $0 \leq \lambda_{mk} < 1$ of the state predictor that are collected in $\Lambda_m = \{\lambda_{m0} = 0, \lambda_{m1}, ..., \lambda_{m4}\}$. Having defined the characteristic polynomial as follows

$$P(\lambda) = \lambda \prod_{k=1}^{4} (\lambda - \lambda_{mk}) = \lambda\left(\lambda^4 + c_{m3}\lambda^3 + c_{m2}\lambda^2 + c_{m1}\lambda + c_{m0}\right), \tag{22}$$

and the unknown polynomial of the state predictor (see equation (24)) as

$$P_m(\lambda, L) = \det\begin{bmatrix} \lambda I - A + N_c LC & -H_c \\ +N_d LC & \lambda - 1 \end{bmatrix}, \tag{23}$$

the gain equations easily follow.

The factor λ in (22) corresponds to the delay (zero eigenvalue, $\lambda_{m0} = 0$) between u and x_0 in (10) and (12). No output feedback closes on $\hat{x}_0$ because it is noise free.

Using the 'hat' notation, the state-predictor equation can be written as

$$\begin{aligned} &\begin{bmatrix} \hat{\mathbf{x}} \\ \hat{x}_d \end{bmatrix}(i+1) = \begin{bmatrix} A - N_c LC & H_c \\ -N_d LC & 1 \end{bmatrix}\begin{bmatrix} \hat{\mathbf{x}} \\ \hat{x}_d \end{bmatrix}(i) + \begin{bmatrix} B \\ 0 \end{bmatrix}u(i) + \\ &+ \begin{bmatrix} N_c L \\ N_d L \end{bmatrix}y(i) + \begin{bmatrix} G \\ 0 \end{bmatrix}v_r(i),\ \begin{bmatrix} \hat{\mathbf{x}} \\ \hat{x}_d \end{bmatrix}(0) = \begin{bmatrix} \hat{\mathbf{x}}_0 \\ \hat{\mathbf{x}}_{d0} \end{bmatrix} \\ &\hat{y}_m(i) = \begin{bmatrix} C & 0 \end{bmatrix}\begin{bmatrix} \hat{\mathbf{x}} \\ \hat{x}_d \end{bmatrix}(i) \end{aligned}, \tag{24}$$

where v_r denotes the same velocity measurement employed in the reference generator.

3.3.2 Design of the state predictor eigenvalues

The design of the state predictor eigenvalues is the key step in the EMC design ([11], [12]). In fact rejection degree and bandwidth of the parametric uncertainties in $\mathbf{h}(\cdot)$ are imposed by the state-predictor sensitivity $\mathbf{S}_m(f)$, whereas the neglected dynamics ∂P is attenuated by the complement $\mathbf{V}_m(f) = 1 - \mathbf{S}_m(f)$. To this end, their product must satisfy the stability inequality

$$\max_{|f| \le f_{\max}} \left| \mathbf{V}(jf)\partial P(jf) \right| \cong \mathbf{V}(jf_{\partial P})\partial P_{\max} \le \eta < 1, \tag{25}$$

where $|\partial P|$ achieves the maximum at $f = f_{\partial P}$. Figure 7 shows the magnitude of both transfer functions.

Consider for simplicity's sake the following parametric uncertainty

$$\mathbf{h}(\mathbf{x}, u, i) = \begin{bmatrix} 0 \\ 0 \\ 0 \\ h_y y_m + h_u u \end{bmatrix} = \begin{bmatrix} 0 \\ 0 \\ 0 \\ \partial R \cdot R y_m / V_{\max} - \partial L u \end{bmatrix}, \tag{26}$$

where h_y accounts for the fractional resistance uncertainty $\partial R < 1$ and h_u for the inductance uncertainty ∂L. In [11] and [12] it has been shown that h_y is attenuated if

$$\begin{aligned} &\max_{|f| \le f_{\max}} \left| \mathbf{S}_m(f)\mathbf{M}(f)h_y \right| \le \eta < 1 \\ &\mathbf{M}(f) = B(e^{j2\pi fT}) / A(e^{j2\pi fT}) \end{aligned}, \tag{27}$$

where A and B are the polynomials in (3) and $1/\eta$ is a stability margin, which may be the same as in (25), since (25) and (27) refer to different frequency bands. Now since $|\mathbf{M}|$ (see Figure 2) is monotonically decreasing and $|\mathbf{S}_m|$ is monotonically increasing in the frequency domain, a unique maximum exists in (27). Using Figure 2 and Figure 7, both magnitudes can be approximated by

$$\left| \mathbf{S}_m(f) \right| \cong f / f_m, \ \left| \mathbf{M}(f) \right| \cong \frac{V_{\max}}{R} f_a / f \tag{28}$$

from 20 Hz to 500 Hz. Thus (27) simplifies to

$$f_m \ge \partial R f_a / \eta, \ f_a \approx 20 \text{ Hz}. \tag{29}$$

By assuming $|\partial R| \le \eta$, (29) provides a moderate lower bound to the state predictor frequency BW f_m in (28). The upper bound to f_m is imposed by (25), and results into

$$\begin{aligned} & f_m \le f_{\partial P}\left(\eta / \partial P_{\max}\right)^{1/r} \cong 450 \text{ Hz} \\ & 0.5 \le r \le 1,\ \eta = 0.4,\ \partial P_{\max} \le 1,\ f_{\partial P} \ge 3000 \text{ Hz} \end{aligned} . \tag{30}$$

The treatment of h_u is more complex as it involves the control law of Section 3.4. In practice (27) must be replaced by

$$\max_{|f| \le f_{\max}} \left|\mathbf{S}_m(f)\mathbf{M}(f)\mathbf{C}(f)h_u\right| \le \eta < 1, \tag{31}$$

where $\mathbf{M}(z)\mathbf{C}(z)$ is the loop transfer function of the control law [11], [12], that in turn defines the sensitivity $\mathbf{S}_c = (1+\mathbf{MC})^{-1}$ and the complement $\mathbf{V}_c = 1 - \mathbf{S}_c$. Since the aim is a deadbeat control, it occurs that $|\mathbf{M}(f)\mathbf{C}(f)| > 1$ from DC to $f_{\max}$, and decays like f_c / f while approaching $f_{\max}$ (the same decay applies to the sensitivity complement $\mathbf{V}_c = 1 - \mathbf{S}_c$). Hence (31) can be replaced by

$$(f / f_m)(f_c / f)h_u \le \eta < 1 \Rightarrow f_m \ge |\partial L| f_c / \eta . \tag{32}$$

Assuming $|\partial L| \approx \eta = 0.4$, inequality (32) is rather critical since it demands that the state-predictor BW f_m is close to the control law BW f_c. Such a demand may conflict with the upper bound in (30), may force f_c to be narrowed, and the dead-beat requirement in (14) to be abandoned. For such reasons solenoid inductance should be accurately known, i.e. $|\partial L| < \eta$, and modeled as a function of I according to Figure 2. Here, to be conservative but in view also of $|\partial L| \le 0.2 < \eta$, all the model parameters in (12) have been assumed to be constant. Their uncertainty and variability are attenuated by $\mathbf{S}_m$ according to (27) and (31).

Figure 7 Harmonic response (magnitude) of the state predictor sensitivity and of the complement.

3.3.3 Comparison with Kalman filter design

It may be of some interest to compare eigenvalue design in the previous section to Kalman filter design. We restrict to a stationary filter that has the same equation as in (24), but is rewritten in the compact form as

$$\begin{aligned}\hat{\mathbf{x}}_p(i+1) &= \left(A_p - LC_p\right)\hat{\mathbf{x}}_p(i) + B_p u(i) + Ly(i),\ \hat{\mathbf{x}}_p(0) = \hat{\mathbf{x}}_{p0} \\ \hat{y}_m(i) &= C_p\hat{\mathbf{x}}_p(i)\end{aligned}. \tag{32}$$

The gain vector L in (21) must be computed as

$$\begin{aligned}L &= \left(A_p PC_p^T + S\right)\left(C_p PC_p^T + r^2\right)^{-1} \\ P &= \left(A_p - LC_p\right)P\left(A_p - LC_p\right)^T + Q + Lr^2L^T - \left(SL^T + LS^T\right)\end{aligned}, \tag{32}$$

where $P \geq 0$ is the state covariance, $r^2 > 0$ is the measurement noise variance, $Q \geq 0$ is the input noise covariance, and $S = 0$ fixes that measurement and input noises are uncorrelated. Comparison is made by fixing the same gain vector L,

$$L = \begin{bmatrix} 0.489 \\ -0.141 \\ 0.00764 \\ 0.0319 \end{bmatrix} \tag{32}$$

hence the same closed-loop eigenvalues in Table I, and thus solving (32) for P and Q, given $S = 0$ and $r = 1$. In this way the results must be scaled by the measurement noise covariance r^2. The matrix equations (32) are linear in the unknowns, but we have to ensure $P \geq 0$ and $Q \geq 0$. First the gain equation in (32) is solved for PC_p^T

$$PC_p^T = \left(A_p - LC_p\right)^{-1} Lr^2. \tag{32}$$

Then the Lyapunov equation is solved for the whole P and Q. Because of the sparsity of A_p, only a pair of diagonal entries of Q, namely $q_{22} = q_{33}$ are iterated for obtaining non negative definite matrices. The input noise covariance matrix results into

$$Q = \begin{bmatrix} 0.14 & -0.068 & -0.010 & 0 \\ -0.068 & 0.033 & 0 & 0 \\ -0.010 & 0 & 0.033 & 0 \\ 0 & 0 & 0 & 0.0018 \end{bmatrix} r^2,\ \det Q = 0 \tag{32}$$

and the square root eigenvalues of Q and P are

$$\begin{aligned} \Lambda(P) &= \{0.084, 0.19, 0.29, 0.91\}\, r \\ \Lambda(Q) &= \{0, 0.042, 0.18, 0.42\}\, r \end{aligned} . \tag{32}$$

As a first remark, the covariance matrix (32) corresponds to an input noise having smaller variance than the measurement noise r^2, which does not agree with the spectral densities of the sensor noise and of $\eta \cong d$ in Figure 4. Indeed, the spectral density of the input noise η is much higher than the sensor noise. As a second remark, one may wonder how practically obtain the matrix Q in (32). Parametric identification in Section 2.2 and disturbance modelling in Section 2.3 have only suggested location and size of the noise vector $\mathbf{w}$ in (10), but no accurate covariance as in (32). The eigenvalue design in Section 3.3.2, typical of Embedded Model Control, fills in the gap.

3.4 Regulator architecture: the control law

The main goal of the control law is to reject the disturbance term $\mathbf{h}(\cdot)$ in (1), which has been modeled by the stochastic disturbance class $\mathcal{D}$ in (7), and to make the closed-loop system approach dead-beat conditions. Following EMC [11], [12] disturbance rejection must satisfy two principles.

1) Only the state variable x_d can enter the control law, unlike w_d, since only the one-step prediction of x_d is made available by the state predictor.
2) When the disturbance input matrix H_c does not belong to the subspace spanned by B (the command input matrix in (12)), an extended tracking error $\underline{\mathbf{e}}$ including the disturbance state x_d must be defined

$$\underline{\mathbf{e}}(i) = \underline{\mathbf{x}}(i) - \mathbf{x}(i) - Q x_d(i) . \tag{33}$$

It has been shown in [28] that only the extended tracking error $\underline{\mathbf{e}}$ can be brought asymptotically to zero, upon a suitable design of the vector Q through a Sylvester-type equation. The same equation has been already found by [29], [30] and [31] in the framework of the internal model principle.

Combining, in accordance with the previous principles, the reference command in (20), the tracking error feedback built on (33) and the disturbance rejection of $\hat{x}_d$, the one-step anticipated duty cycle takes the following form:

$$\begin{aligned} u_c(i+1) &= \underline{u}(i+1) + K\left(\underline{\mathbf{x}}(i+1) - \hat{\mathbf{x}}(i+1) - Q\hat{x}_d(i+1)\right) - m\hat{x}_d(i+1) \\ u(i+1) &= \mathrm{sat}\left(u_c(i+1) + u_0\right) \end{aligned}, \tag{34}$$

where $\mathrm{sat}(\cdot)$ denotes saturation to the duty-cycle limits in (16), and $u_0 = V_0 / V_{\max}$ is the duty cycle offset. Finally Q and m satisfy the following Sylvester-type equation

$$\begin{bmatrix} H_c + Q \\ 0 \end{bmatrix} = \begin{bmatrix} A & B \\ C & 0 \end{bmatrix} \begin{bmatrix} Q \\ m \end{bmatrix}. \tag{35}$$

One-step anticipation in (34) is compulsory for recovering the computing delay. Anticipation is permitted by the one-step predictor in (24).

The gains of the row vector $K = \begin{bmatrix} k_3 & k_2 & k_1 & k_0 \end{bmatrix}$ are obtained in a way similar to L, i.e. by fixing the eigenvalues $\Lambda_c = \{\lambda_{c0}, ..., \lambda_{c3}\}$ of the closed-loop matrix $A - BK$.

The eigenvalues of the embedded model, of the state predictor and of the control law are reported in Table I. The control-law eigenvalues are the same as the open-loop ones, except for a single eigenvalue, $\lambda_{c3} = 0.52$, which is in charge of widening the BW up to about $f_c \cong 800$ Hz for approaching dead-beat conditions. A pair of state predictor eigenvalues $\lambda_{m3} = 0.7,\ \lambda_{m4} = 0.8$ are free, and are fixed not far from f_c (one octave below) so as to respect the critical inequality (32).

Table I -Open-loop and closed loop eigenvalues.

The commanded duty cycle u in (34), when converted to a voltage $V(t)$, $|V(t)| \le V_{\max}$, must include the nominal voltage offset V_0 in (17), and reads as

$$V(t) = V_0 + u(t)V_{\max}. \tag{36}$$

4 Experimental results and discussion

Experimental results aim to verify the requirements in (14).

4.1 Slew rate

The slew rate, tested through a square-wave reference current, appears to compatible with values in (17). Figure 8 shows the current reference (10 Hz square wave) and the measured current response. The increasing current jump tracks the reference more slowly than the decreasing leg, because of the asymmetrical voltage limits in (17) as in Figure 10. Figure 9 shows the response to a decreasing current jump, which requires a negative voltage jump and thus benefits from the larger slew rate in (17). Figure 10 shows the commanded voltage $V(t)$ defined in (36). The dashed curve, $V_{nom} = \underline{u} V_{\max}$, is the nominal command (in voltage units) computed by the reference generator in (18) and (20).

Figure 8 Reference and response to a 10-Hz square wave.

Figure 9 Response to a decreasing current jump (enlargement of Figure 8).

Figure 10 Commanded duty cycle converted to voltage.

4.2 Delay and tracking accuracy

The dead-beat equation (14) has been tested in the time and frequency domains. Magnitude and argument of the harmonic response are shown in Figure 11 and Figure 12. They are compared with an existing analogue current regulator, showing significant improvement. The response approaches a delay of 0.2 ms, which is smaller than the bound in (14), and equal to the open-loop relative degree. As a proof, the argument of a 0.2 ms delay fits the experimental argument as shown by Figure 12. Figure 12 further shows that the closed-loop argument has been increased from the open-loop profile in Figure 3 only in the mid frequency domain, i.e. below 1 kHz. This further proves that the relative degree is $n+1-m=2$, and is maintained as expected by the closed-loop dynamics.

Figure 11 Harmonic response of the current regulator (digital and analogue): magnitude.

Figure 12 Closed-loop (digital and analogue) and open-loop harmonic response: argument.

The measured tracking error y_e is the combination of the nominal error $\underline{e}_{nom}$ in (14) which is imposed by the 0.2 ms delay and of the residual $\underline{e}_{res}$ of the disturbance rejection. The error expression can be obtained by rewriting (14) as follows

$$\begin{aligned} y_e(t) &= \underline{I}(t) - I(t) = \underline{I}(t) - \underline{I}(t-\tau) - \underline{e}(t) = \underline{e}_{nom} + \underline{e}_{res}(t) \\ \underline{e}_{res}(t) &= -\underline{e}(t) \end{aligned} \tag{37}$$

Figure 13 shows the nominal and the measured tracking error in response to a 10-Hz triangular wave having a 12 A/s slew rate and a magnitude of ± 0.3 A around the current offset. The transient and steady state residuals remain below the 1.5 mA threshold of (14), but show a peak (high frequency) and a drift (mid frequency) because of the variable inductance, that the disturbance $\hat{x}_d$ cannot completely reject. This is the intrinsic limitation of any unknown disturbance estimation as in (24) and of any rejection as in (34), as they suffer from the upper bound (30) on the state predictor BW. Only a more accurate model around $f \approx f_m$ can loose the restraint.

Figure 13 Nominal and measured tracking error in response to a triangular wave.

Figure 14 repeats Figure 13 for a 10-Hz sine wave having a slew rate of 38 A/s and a magnitude of ± 0.3 A around the current offset. The residuals (total error minus nominal) still remain below the target of 1.5 mA.

Figure 14 Nominal and measured tracking error in response to a sine wave.

4.3 Disturbance rejection

The benefits of complementing the electromotive force compensation (reference generator) with an unknown disturbance estimation can be appreciated in Figure 15 and Figure 16. In both cases (the current varies of ± 0.3 A around the offset) the disturbance magnitude is of the same order of the tracking error residuals, but they allow the systematic component of the error to be reduced.

Figure 15 Total rejected disturbance and components in response to a triangular wave.

Figure 16 Total rejected disturbance and components in response to a square wave.

To illustrate the benefit of the unknown disturbance estimate, the electromotive force has been underestimated by a factor of about 0.5, but the unknown disturbance recovers the error and completes the disturbance estimate with other components, that are not referable to the electromotive force. That increases regulator robustness, and guarantees the target accuracy in (14).

5 Conclusions

The paper has shown how unknown disturbance rejection can improve the robustness of a simple but ubiquitous control system like a current regulator. A linear time-invariant model and the estimation of the parametric uncertainties through a simple stochastic dynamics do the task. The solenoid of an electro-hydraulic valve was the study case. The current regulator presented in this paper is the inner wide-band loop of a proportional valve position control.

6 Acknowledgments

The authors are grateful to anonymous reviewers for their useful remarks and suggestions. Part of the work of the authors from Politecnico di Torino has been supported by a grant from Atos SpA, Sesto Calende, Italy.

7 References

[1] R. Krishnan, *Electric motor drives modeling, analysis and control,* Prentice-Hall, New Jersey, 2001.

[2] L. A. Mianzo, S. J. Newton and Z. Popovic "Integrated control and power electronics for an electro-mechanical valve actuation system", *Proc. Int. Conf. on Advanced Intelligent Mechatronics*, Monterey, CA, 24-28 July 2005, pp.485-491.

[3] H-Z. Jin and J-M. Lee "An RMRAC current regulator for permanent magnet synchronous motors based on statistical model interpretation", *IEEE Trans. Industrial Electronics*, Vol. 56, No. 11, 2009, pp. 169-177.

[4] C-Y. Chen, W-C. Chan, T-C. Ou, S-H. Yu, and T-W Liu "Sliding mode speed control of brushless DC motor using Pulse-Width Modulated current regulator", *2009 IEEE/ASME Int. Conf. on Advanced Intelligent Mechatronics,* Singapore, July 14-17, 2009, pp. 1395-1399.

[5] H-Z Jin and J-M. Lee "A novel adaptive current regulator for permanent magnet synchronous motor based on modified current dynamics", *Proc. IEEE International Conf. in Industrial Informatics (INDIN 2008),* Daejeon, Korea, July 13-16, pp. 927-932.

[6] H. Kim, M.W. Degner, J. M. Guerrero, F. Briz, and R. D. Lorenz "Discrete-time current regulator design for AC Machine Drivers", *IEEE Trans. Industrial Applications,* Vol. 46, No. 4, 2010, pp. 1425.

[7] D.G. Holmes, B. P. McGrath and S. G. Parker "Current regulation strategies for vector-controlled induction motor drives", *IEEE Trans. Industrial Electronics*, Vol. 59, No. 10, 2012, pp. 3680-3689.

[8] J. Zhou and W. Dehaene "Fully integrated CMOS EME-suppressing current regulator for automotive electronics", *IEEE Trans. Circuit and Systems,* Vol. 59, No. 2, 2012, pp. 266.

[9] P. Wang, F-S. Liu and X-R Li "Driving characteristics for electronic control unit pump fuel injection system", *Proc. 2012 IEEE Int. Conf. on Computer Distributed Control and Intelligent Environmental Monitoring,* 2012, pp. 264.

[10] H.G. Jung, J.Y. Hwang, P.J. Yoon and J. H. Kim "Robust solenoid current control for EHB", *2005 SAE World Congress,* Detroit, Michigan, April 11-14, 2005, SAE Technical Paper Series 2005-01-1583.

[11] E. Canuto, W. Acuna-Bravo, A. Molano and C. Perez "Embedded Model Control calls for disturbance modeling and rejection", *ISA Transactions*, Vol. 51, No. 5, 2012, pp. 584-595.

[12] E. Canuto, W. Acuna-Bravo and C Perez "Robust control stability using the error loop", *Int. J. of Mechatronics and Automation*, Vol. 3 No. 2, 2013, pp. 94-109.

[13] E. Canuto and W. Acuna-Bravo "Hierarchical digital control of a proportional electro-hydraulic valve", *Proc. 2013 IEEE Conference on Mechatronics and Automation*, Takamatsu, Japan, August 4-7, 2013, pp. 1015-1020.

[14] B.P. McGrath, S.G. Parker and D.G. Holmes, "High performance stationary frame AC current regulation incorporating transport delay compensation", *Proc. of the 14th European Conf. on Power Electronics and Applications (EPE 2011),* 2011, pp.1-10.

[15] B. Lequesne "Dynamic model of solenoid under impact excitation, including motion and eddy currents", *IEEE Trans. on Magnetics*, Vol. 26, No. 2, 1990, pp. 1107-1116.

[16] Z. Gao "Active disturbance rejection control: a paradigm shift in feedback control system design", *Proc. 2006 American Control Conf,* 2006, pp. 1399-2405.

[17] J. Han "From PID to active disturbance rejection control", *IEEE Trans. on Industrial Electronics,* Vol. 56, 2009, pp. 900-906.

[18] G. Jung, J. Y. Hwang, P. J. Yoon and J.H. Kim "Resistance estimation of PWM-driven solenoid", *Int. J. of Automotive Technology*, Vol. 6, No. 2, 2007, pp. 249-258.

[19] M. Ruderman, A. Ruderman and T. Bertram "Observer-based compensation of additive periodic torque disturbances in permanent magnet motors", *IEEE Trans. Industrial Informatics*, Vol. 9, No. 2, 2013, pp. 1130-1138.

[20] S. Li, J. Kung, W-H. Chen and X Chen "Generalized extended state observer based control for systems with mismatched uncertainties", *IEEE Trans. Industrial Electronics*, Vol. 59, No. 12, 2012, pp. 4792-4802.

[21] J. Ospina, E. Canuto, A. Molano Jimenez and W. Acuna-Bravo "Multilayer Control of an Optical Reference Cavity for Space Applications", *IEEE Trans. Industrial Electronics*, Vol. 57, No. 7, 2010, pp. 2507-2518.

[22] E. Canuto, F. Musso and J. Ospina "Embedded Model Control: Submicroradian Horizontality of the Nanobalance Thrust-Stand", *IEEE Trans. Industrial Electronics*, Vol. 57, No. 7, 2010, pp. 2507-2518.

[23] S-N. Yun, Y-B. Ham and J-Ho Park "New approach to design control cone for electro-magnetic proportional solenoid actuator", *Proc. 2012 IEEE/ASME Int. Conf. on Advanced Intelligent Mechatronics*", July 11-14, 2012, Kaohsiung, Taiwan, pp. 982-987.

[24] T. Soderstrom and P. Stoica, *System Identification*, Prentice-Hall, New York, 1989.

[25] L. Ljung, *System Identification, Theory for the user*, 2nd ed., Prentice-Hall, Upper Saddle Hall, NJ, 1999.

[26] E. Canuto, J. Ospina and W. Acuna-Bravo "Dynamic and relative calibration of temperature sensors in the case of uncertain parameters", *Zhongguo Kexue Jishu Daxue Xuebao*, vol. 42 n. 5, 2012, pp. 345-356.

[27] E. Canuto, A. Molano and L. Massotti "Drag-free control of the GOCE satellite: noise and observer design", *IEEE Trans. Control Systems Technology,* Vol. 18, No. 2, 2010, pp. 501-509.

[28] E. Canuto "Embedded Model Control: outline of the theory", *ISA Transactions*, Vol. 46, No. 3, 2007, pp. 363-377.

[29] E. Davison "The output control of linear time invariant multivariable systems with unmeasurable arbitrary disturbances", *IEEE Trans. Automatic Control*, Vol. 17, No. 5, 1972, pp. 621-630.

[30] E. Davison "The robust control of a servomechanism problem for linear time-invariant multivariable systems", *IEEE Trans. Automatic Control*, Vol. 21, No. 1, 1976, pp. 25-34.

[31] B.A. Francis "The internal model principle of control theory", *Automatica,* Vol. 12, No. 5, 1976, pp. 457-465.

To appear in ISA Transactions, DOI: 10.1016/j.isatra.2013.08.013

Figures and tables

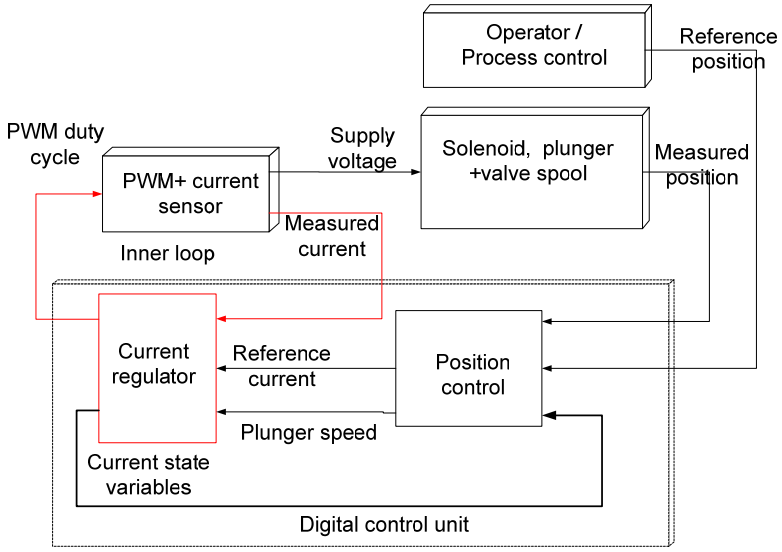

Figure caption 1. Current regulator and position control.

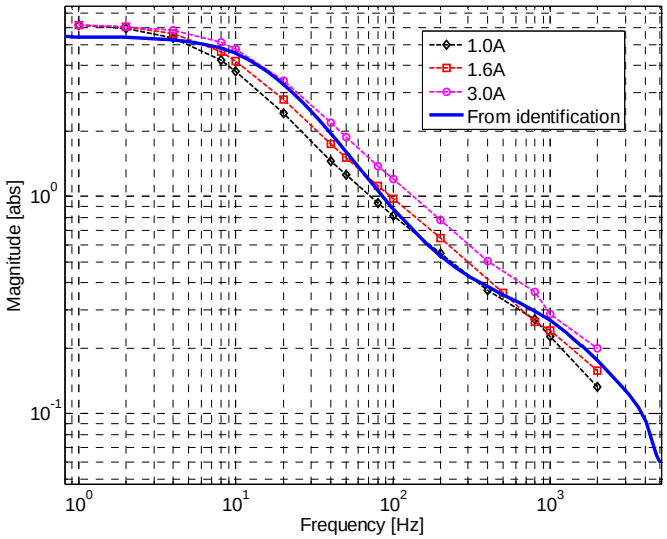

Figure caption 2. Magnitude of the harmonic response.

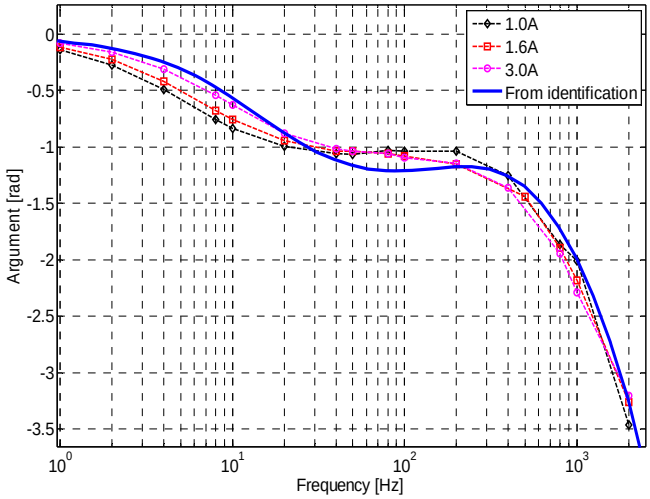

Figure caption 3. Argument of the harmonic response.

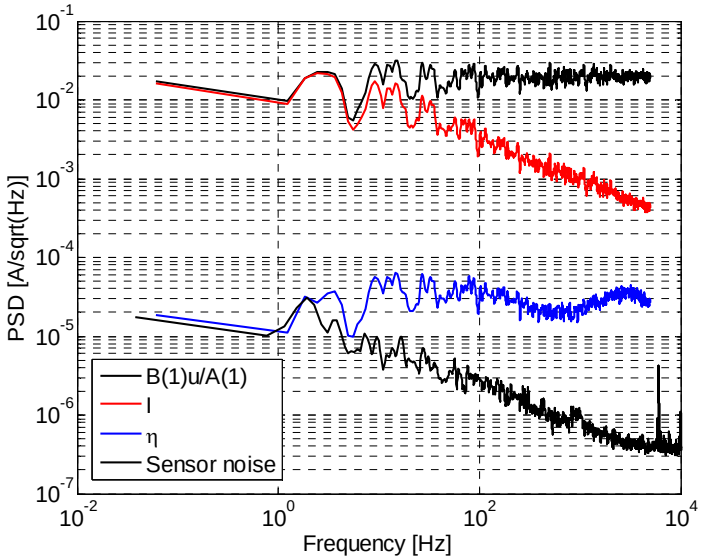

Figure caption 4. Spectral density of the normalized duty cycle (top), of the measured current (decreasing curve), of the residuals (middle) and of the sensor noise (bottom).

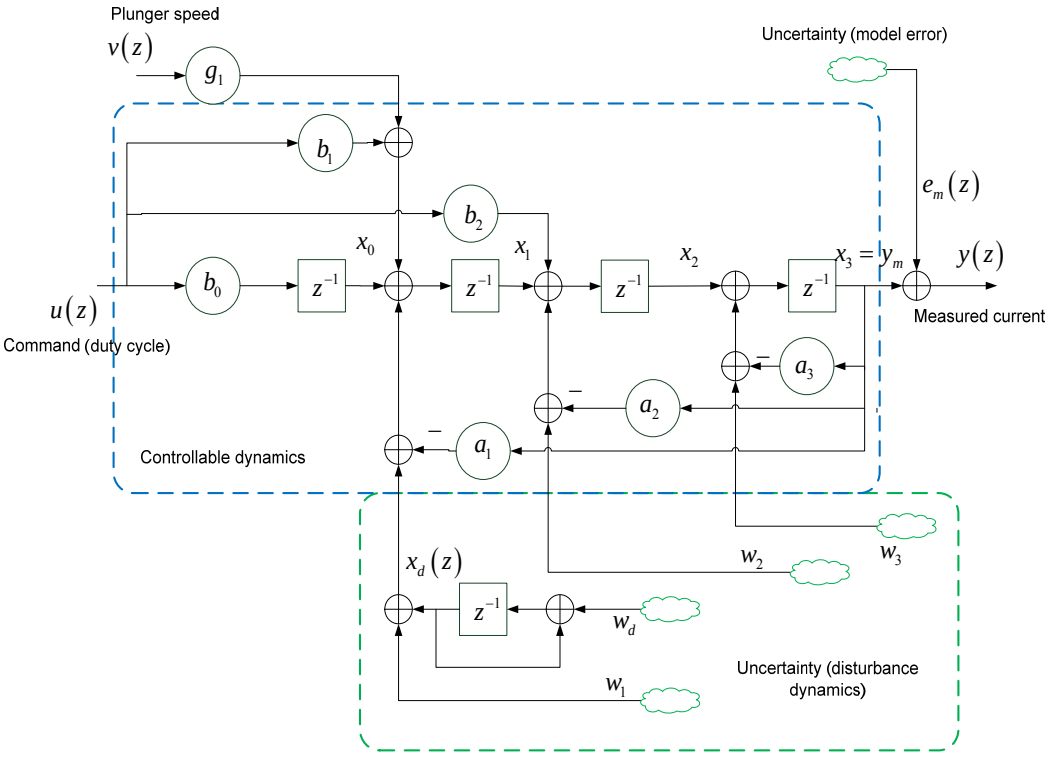

Figure caption 5. Block-diagram of the embedded model.

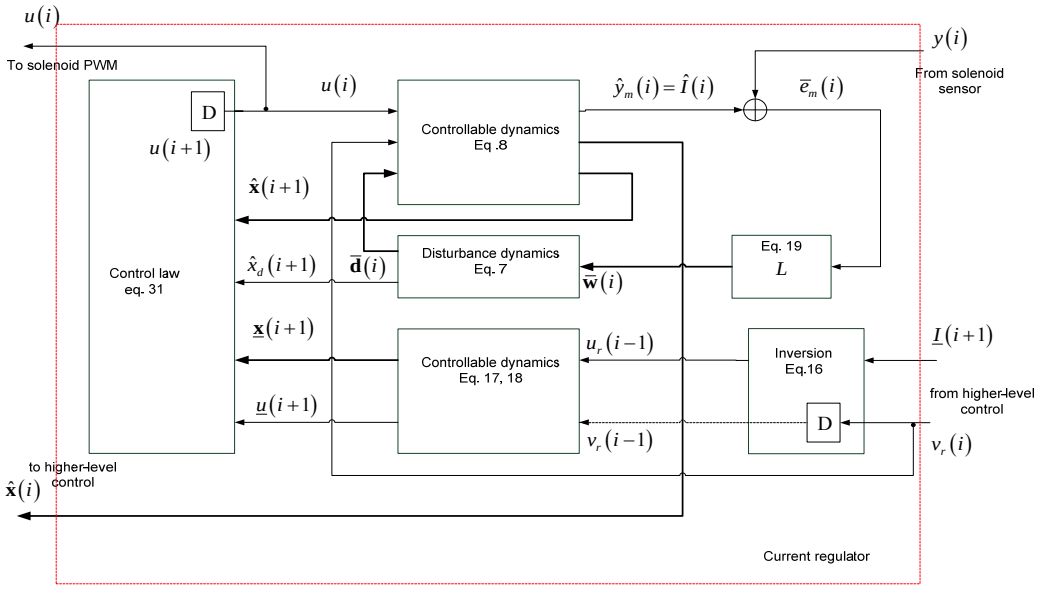

Figure caption 6. Current regulator block-diagram.

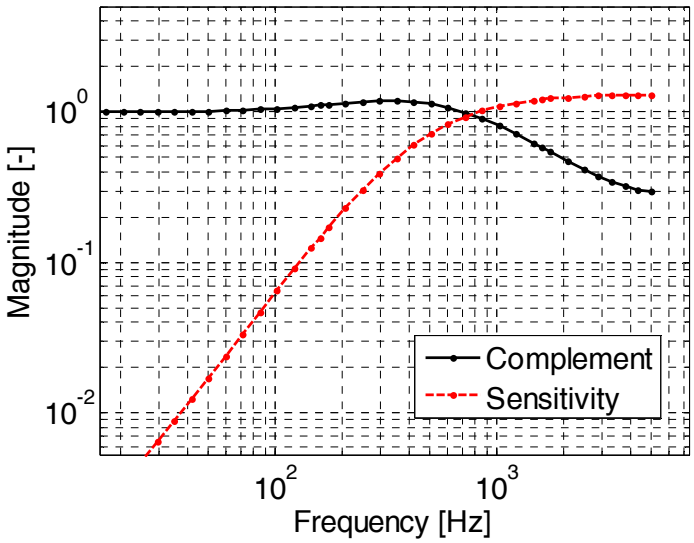

Figure caption 7. Harmonic response (magnitude) of the state predictor sensitivity and of its complement.

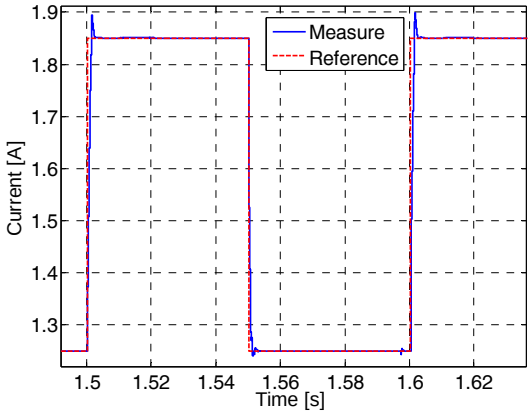

Figure caption 8. Reference and response to a 10-Hz square wave.

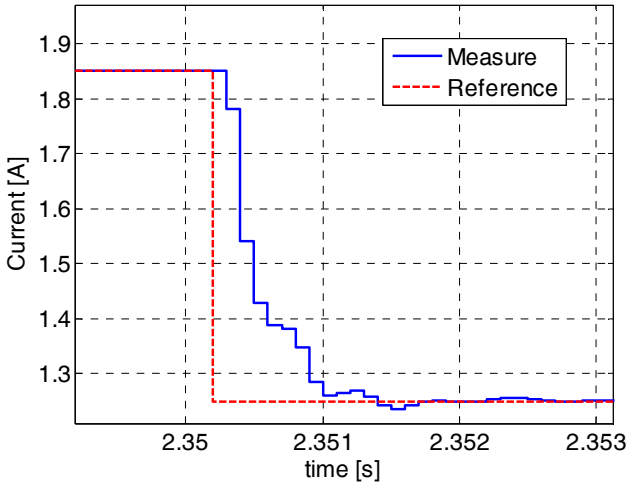

Figure caption 9. Response to a negative current jump.

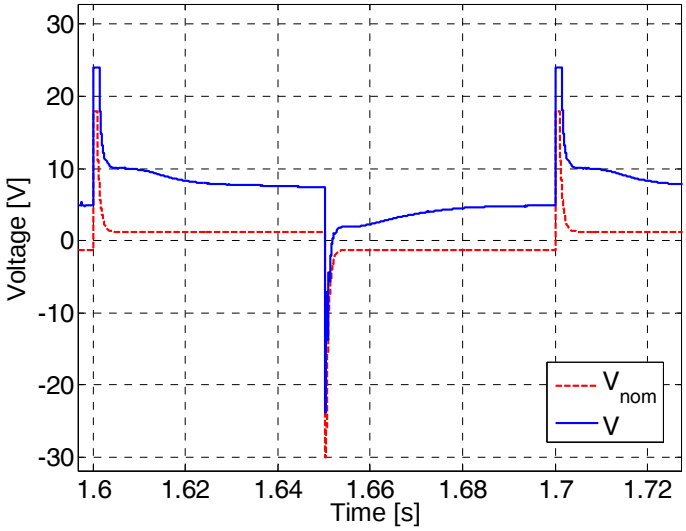

Figure caption 10. Commanded duty cycle converted to a voltage signal.

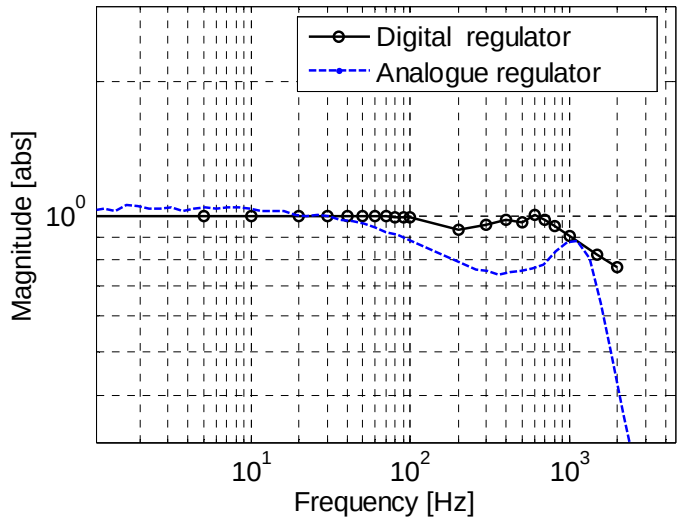

Figure caption 11. Harmonic response of the current regulator (digital and analogue): magnitude.

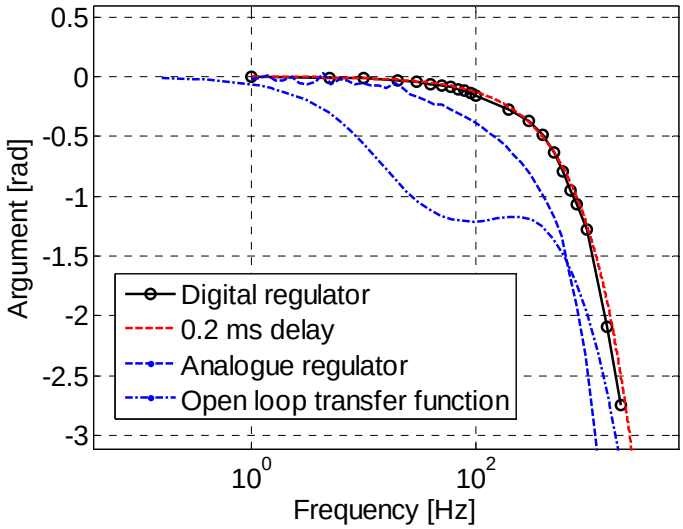

Figure caption 12. Closed-loop (digital and analogue) and open-loop harmonic response: argument.

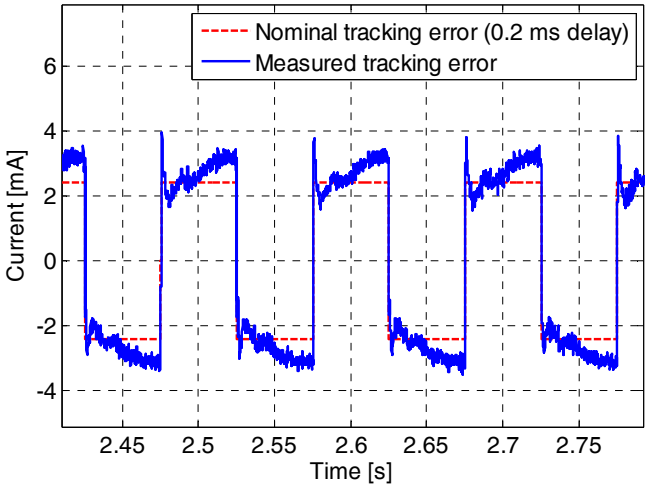

Figure caption 13. Nominal and measured tracking error in response to a triangular wave.

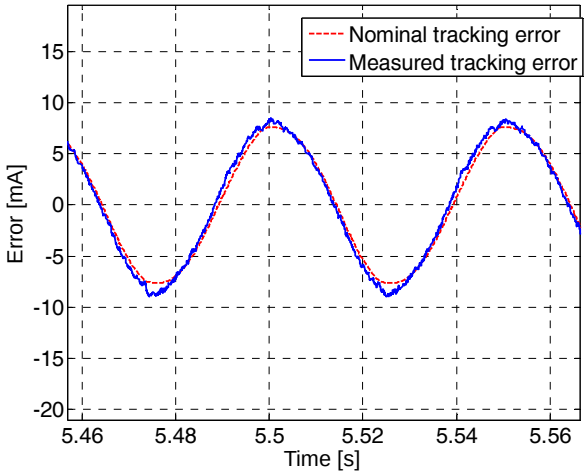

Figure caption 14. Nominal and measured tracking error in response to a sine wave.

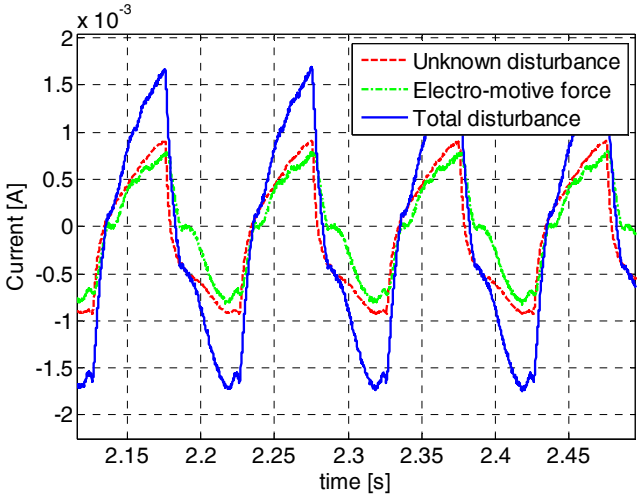

Figure caption 15. Total rejected disturbance and components in response to a triangular wave.

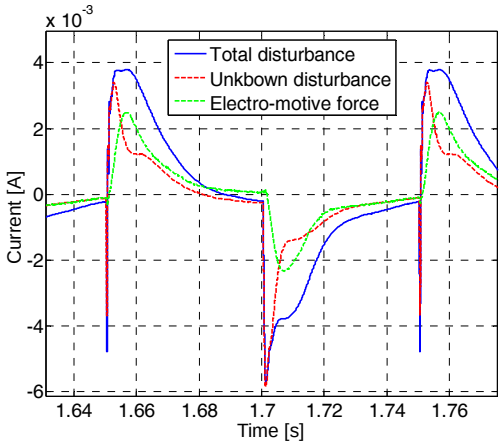

Figure caption 16. Total rejected disturbance and components in response to a square wave

Table I Open-loop and closed loop eigenvalues

No.	Equation	BW	Eigenvalues
0	Embedded model	$f_a \cong 20$ Hz	0, -0.1, 0.52, 0.989
1	State predictor	$f_m \cong 400$ Hz	0, -0.1, 0.52, 0.7, 0.8
2	Control law	$f_c \cong 800$ Hz	0, -0.1, 0.52, 0.52